

# Anion-Containing Solvation Structure Reconfiguration Enables Wide-Temperature Electrolyte for High-Energy-Density Lithium-Metal Batteries

Silan Kuang, Haiming Hua, Pengbin Lai, Jialin Li, Xiaodie Deng, Yang Yang,\* and Jinbao Zhao\*



Cite This: *ACS Appl. Mater. Interfaces* 2022, 14, 19056–19066



Read Online

ACCESS |



Metrics & More



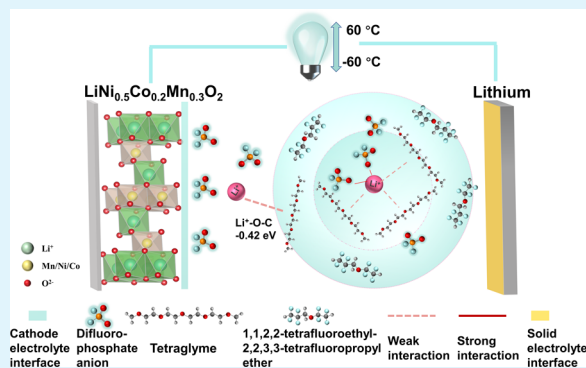
Article Recommendations



Supporting Information

**ABSTRACT:** The demand for high-energy-density lithium batteries (LBs) that work under a wide temperature range ( $-40$  to  $60$  °C) has been increasing recently. However, the conventional lithium hexafluorophosphate ( $\text{LiPF}_6$ )-based ester electrolyte with a solvent-based solvation structure has limited the practical application of LBs under extreme temperature conditions. In this work, a novel localized high-concentration electrolyte (LHCE) system is designed to achieve the anion-containing solvation structure with less free solvent molecules using lithium difluorophosphate ( $\text{LiPO}_2\text{F}_2$ ) as a lithium salt, which enables wide-temperature electrolyte for LBs. The optimized solvation structure contributes to the cathode–electrolyte interface (CEI) with abundant  $\text{LiF}$  and  $\text{P-O}$  components on the surface of the  $\text{LiNi}_{0.5}\text{Co}_{0.2}\text{Mn}_{0.3}\text{O}_2$  (NCM523) cathode, effectively inhibiting the decomposition of electrolyte and the dissolution of transition-metal ions (TMIs). Moreover, the weakened  $\text{Li}^+$ –dipole interaction is also beneficial to the desolvation process. Therefore, the 4.3 V  $\text{Li}|\text{NCM523}$  cell using the modified electrolyte maintains a high capacity retention of 81.0% after 200 cycles under  $60$  °C. Meanwhile, a considerable capacity of  $70.9 \text{ mAh g}^{-1}$  (42.0% of that at room temperature) can be released at an extremely low temperature of  $-60$  °C. This modified electrolyte dramatically enhances the electrochemical stability of NCM523 cells by regulating the solvation structure, providing guidelines for designing a multifunctional electrolyte that works under a wide temperature range.

**KEYWORDS:**  $\text{LiPO}_2\text{F}_2$ , localized high-concentration electrolyte, solvation structure, wide temperature, high voltage



## 1. INTRODUCTION

With the booming development of 3C digital devices and electric vehicles (EVs), there is a huge demand for higher-density batteries working under a wide temperature range ( $-40$  ~  $60$  °C),<sup>1,2</sup> such as cold regions and hot desert conditions.<sup>3</sup> Lithium-metal batteries with commercial  $\text{Li-Ni}_x\text{Co}_y\text{Mn}_{1-x-y}\text{O}_2$  (NCM) materials as cathodes are considered to be one of the most promising battery technologies due to the intrinsic high specific capacity and a high working voltage.<sup>4</sup> However, the practical application of  $\text{Li}|\text{NCM}$  batteries has been greatly limited especially under high temperatures ( $>50$  °C) or high operating voltages ( $>4.3$  V)<sup>5</sup> due to the unstable CEI caused by the parasitic reaction of  $\text{LiPF}_6$ -based ester electrolyte.<sup>6–8</sup> In addition, the low-temperature electrochemical performance has been hampered by solvents with high freezing point and strong binding energy with  $\text{Li}^+$  such as EC ( $36.4$  °C).<sup>9,10</sup>

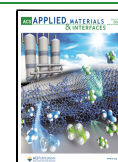
Electrolytes that operate under a wide temperature range and high voltage have been extensively studied by many scientists to improve the wide-temperature cycling performance of lithium batteries.<sup>2,11–14</sup> Examples include the optimization of electrolyte components,<sup>15</sup> the regulation of

the electrode–electrolyte interface (EEI),<sup>16–18</sup> and designing a novel liquefied gas electrolyte.<sup>19,20</sup> Among them, the regulation of the solvation structure is essential and challenging.<sup>21–23</sup> The solvation sheath around  $\text{Li}^+$  determines the composition of CEI<sup>24,25</sup> and desolvation process,<sup>26</sup> which affects the wide-temperature performance of the batteries. The lithium salt determines the essential properties and anion species of electrolyte,<sup>27,28</sup> becoming a key factor affecting the solvation structure. Pham et al.<sup>29</sup> reported that  $\text{Li}^+$ – $\text{PO}_2\text{F}_2^-$  interaction is stronger than  $\text{Li}^+$ –solvents interaction, generating more contact ion pairs (CIPs) and cation–anion aggregates (AGGs). The CIPs and AGGs are favorable for the formation of CEI and SEI full of inorganic components.<sup>30,31</sup> In addition, Shang guan et al.<sup>32</sup> certified that  $\text{LiDFP}$  can generate inorganic

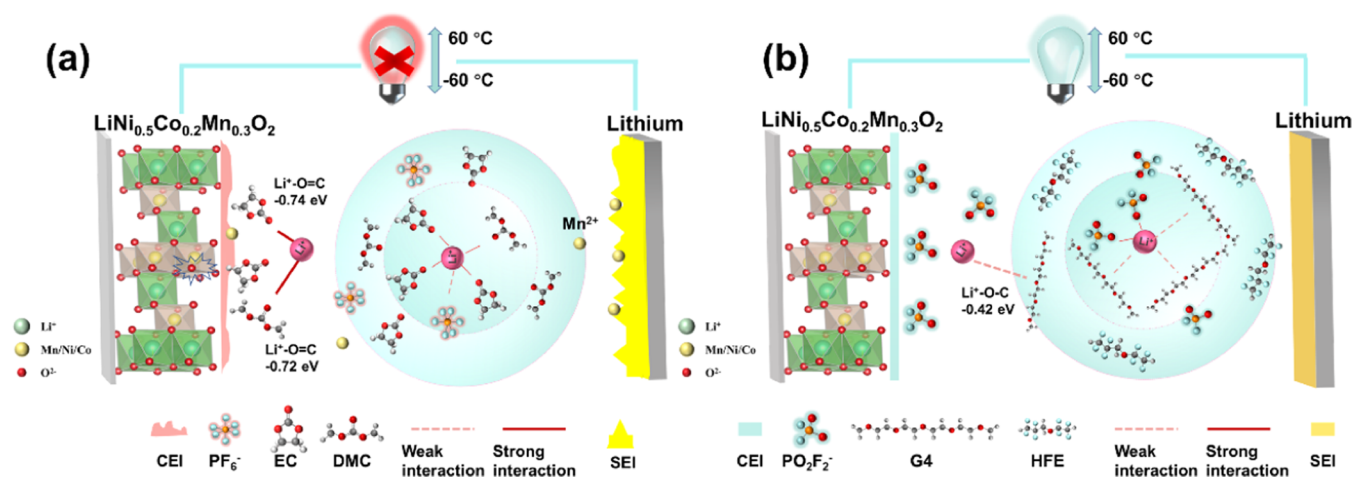
**Received:** February 10, 2022

**Accepted:** April 4, 2022

**Published:** April 14, 2022



Scheme 1. Illustration of the Solvation Structure and the Interfacial Chemistry at the Cathode–Electrolyte Interface in (a) 301 and (b) 1.4M LG\*



substances such as P–O and LiF on the surface of the positive electrode, enabling the electrochemical performance of Lill NCM523 under a wide temperature range ( $-40$  to  $90$  °C). Furthermore, Placke's group pointed out that LiDFP can capture the dissolved TMIs, reducing the crosstalk phenomenon of the NCM523 cathode and the lithium anode.<sup>33–35</sup> However, the strong interaction of  $\text{Li}^+$  and  $\text{PO}_2\text{F}_2^-$  may improve the number of free solvents,<sup>22</sup> affecting the interfacial reaction. Using a high-concentration electrolyte (HCE) is a good way to reduce free solvents, maintain CIPs and AGG structure, and widen the voltage window.<sup>36,37</sup> An increase in lithium salt leads to more anions instead of solvents in the primary sheath of the electrolyte, enabling a stable CEI<sup>30</sup> and accelerating the desolvation process.<sup>10</sup> However, the commercial application of HCE is limited by its high viscosity and high cost.<sup>37</sup> Then, inert solvents such as 1,1,2,2-tetrafluoroethyl-2,2,3,3-tetrafluoropropyl ether (HFE) are introduced into HCE for dilution.<sup>38</sup> The formed localized-concentration electrolyte (LHCE) contains lower viscosity and maintains similar microstructure and physicochemical properties to HCE.<sup>39</sup> As shown in Table S1, LiDFP-based LHCE improves the wide-temperature performance of Lill NCM523 cells. Nevertheless, the solvation structure of LiDFP-based LHCE and its working mechanism on the cathode interface under challenging conditions remains to be explored.

In this work, LiDFP and tetraglyme (G4) with a high boiling point ( $275$  °C) and a low freezing point ( $-40$  °C) were used to design an LHCE (1.4M LiDFP-G4/HFE). Theoretical calculations and  $^7\text{Li}$ -NMR are combined to simulate the solvation structure around  $\text{Li}^+$ , and commercial 1M  $\text{LiPF}_6$ –EC/DMC (1:1 wt %) (301) is used for comparison (Scheme 1). In the 301 electrolyte, the interaction between  $\text{Li}^+$  and EC and DMC is stronger than that with  $\text{PF}_6^-$  in the primary solvation sheath,<sup>40</sup> with slow  $\text{Li}^+$  desolvation.<sup>10</sup> During the discharge process, solvent molecules are enriched on the positive electrode, resulting in an uneven CEI and more MIT dissolution. Nevertheless, in a modified electrolyte (1.4M LGH\*), the first solvation sheath is mainly dominated by anions and solvent molecules are weakly bound to lithium ions instead of being free. The  $\text{PO}_2\text{F}_2^-$  can help generate a uniform CEI full of inorganic components (P–O, LiF) on the positive electrode interface, which is beneficial to the high-temperature or high-voltage cycling of the batteries. In addition, the weak

interaction between  $\text{Li}^+$  and G4 can accelerate the desolvation process, improving the low-temperature discharge capacity.

## 2. EXPERIMENTAL SECTION

### 2.1. Preparation of Materials.

The commercial electrolyte 1 M  $\text{LiPF}_6$  EC/DMC (1:1 wt %) (301) was purchased from Guotai-Huarong Company. Other electrolytes are self-contained. First, electrolytes with 1–6 mol  $\text{L}^{-1}$  concentrations were formed by adding 1–6 mol salt into 1 L of solvent. Then, 1,1,2,2-tetrafluoroethyl-2,2,3,3-tetrafluoropropyl ether (HFE) was added to dilute 4 M LiDFP-G4 (4 M LG), according to a molar ratio of  $n_{\text{LiDFP}}:n_{\text{HFE}} = 1:x$  ( $x = 1, 1.5, 2$ ). All electrolytes were stirred under  $60$  °C. The LHCEs were named 2M LGH, 1.6 M LGH, and 1.4M LGH. 5%FEC additive was added to 1.4M LGH, named 1.4M LGH\*. The locking-field electrolyte of  $^7\text{Li}$ -NMR was  $0.1$  mol  $\text{L}^{-1}$   $\text{LiClO}_4\text{-D}_2\text{O}$ .

NCM523 active material (provided by Beijing Easpring Material Technology Co., Ltd. (China)), acetylene black, and poly(vinylidene fluoride) (PVDF) (8:1:1) were used to prepare the NCM523 cathode. Then, *N*-methylpyrrolidone (NMP) was used as a dispersing agent. The slurry was stirred in a blender for 1 h and then poured onto an aluminum (Al) foil by an automatic coating machine. The coated Al foil was baked at  $80$  °C for 1.5 h. Finally, the sheet was transferred to a  $80$  °C vacuum oven for 24 h. The NCM523 plates had a diameter of 12 mm and a loading density of  $3.0$  mg  $\text{cm}^{-2}$  ( $0.48$  mAh  $\text{cm}^{-2}$ ). The lithium foil had a thickness of 1 mm and a diameter of 14 mm. The method of preparing the SP-PVDF-Al electrode was the same as that used for the cathode material above, without an active substance.

### 2.2. Theoretical Calculations.

The DFT (density functional theory) calculation of HOMO and the lowest unoccupied molecular orbital (LUMO) in this work was run on the Gaussian09 software package,<sup>41</sup> using the B3LYP<sup>42</sup> method at the 6-311+G (d, p) basis set<sup>43,44</sup> to optimize the geometry structure. The solvent environment of the molecule was described in the SMD implicit solvation model.<sup>45</sup> Tetrahydrofuran (Dielectric Constant 7.57) and acetone (Dielectric Constant 20.49) were used as the solvent to calculate the binding energy of G4 and carbonate solvent, respectively, for their similar dielectric constant.<sup>6</sup> The binding energy ( $E_b$ ) between solvents and lithium ions was calculated by the following equation

$$E_b = E_{\text{total}} - E_{\text{Li}^+} - E_{\text{sol}} \quad (1)$$

where  $E_b$  is the binding energy of lithium ion with the solvent and  $E_{\text{total}}$  is the total system's single point energy.  $E_{\text{Li}^+}$  is the  $\text{Li}^+$  ion's single point energy and  $E_{\text{sol}}$  is the solvent's single point energy.

All molecular dynamics simulations were performed by employing Gromacs 2018<sup>46</sup> software. Three concentrations of the solution were simulated, and their ratios are given in Table S2. We chose the OPLS-

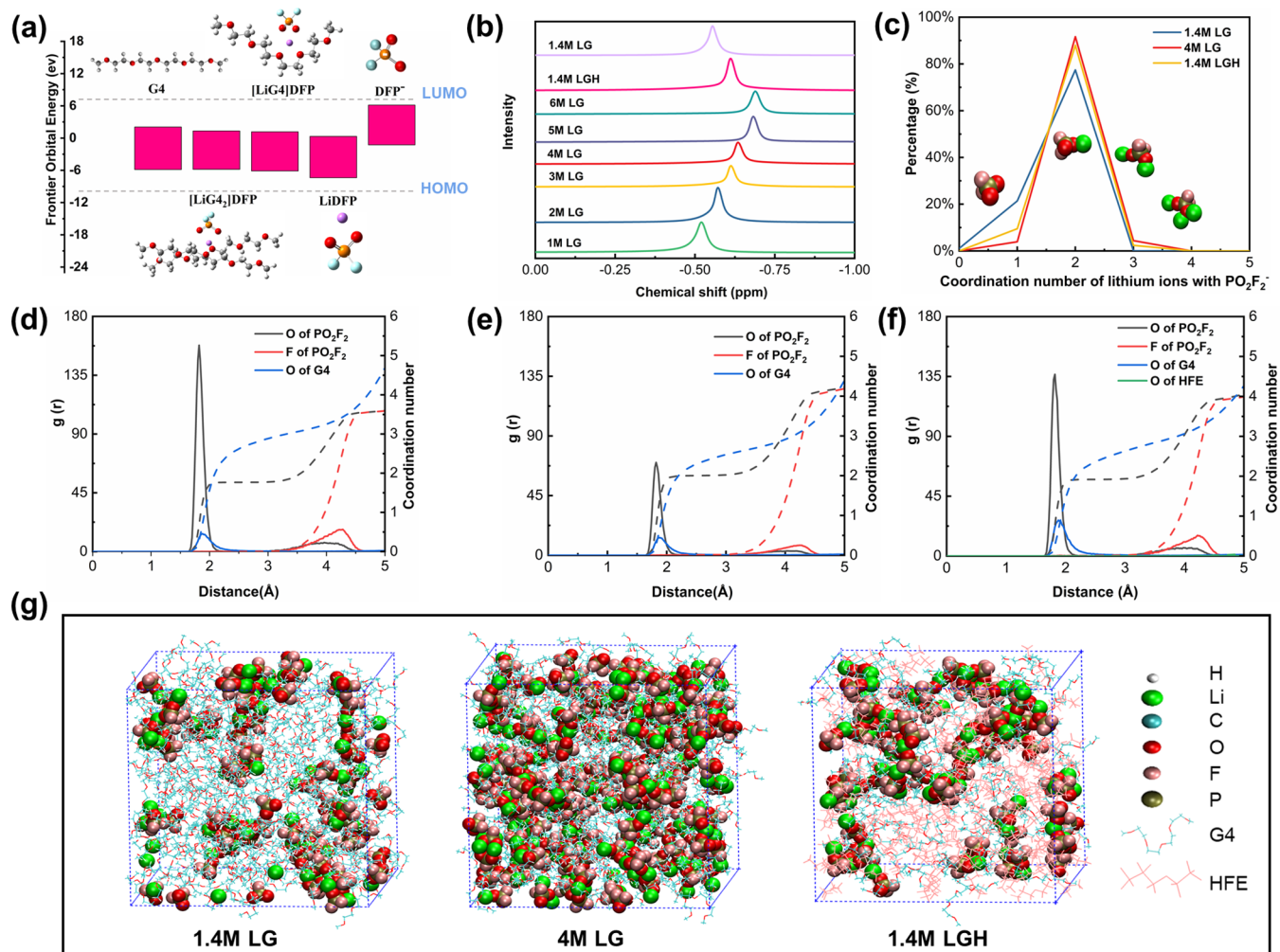


**Figure 1.** Physicochemical properties of different electrolytes. (a) LUMO and HOMO energy levels were calculated by DFT (25 °C). (b)  $^7\text{Li}$ -NMR spectra of electrolytes of different concentrations. (c) Association of  $\text{PO}_2\text{F}_2^-$  with  $\text{Li}^+$ . Radial distribution functions (RDFs) of (d) dilute electrolyte (1.4M LG), (e) HCE (4M LG), and (f) LHCE (1.4M LGH). (g) Molecular dynamics (MD) simulation snapshots of the three electrolytes (1.4M LG, 4M LG, 1.4M LGH).

AA force field,<sup>47</sup> which is suitable for an electrolyte solution. The force field parameters of each molecule were taken from the literature.<sup>48–50</sup> Atomic charges of ions were multiplied by a scale factor of 0.78 to correct the polarization effect of anions and cations.<sup>51</sup>

A simulation box was built by the Packmol software<sup>52</sup> and then submitted to energy minimization using the conjugate gradient method. The equilibrium simulation was carried out with the NPT ensemble at 298.2 K and 1 bar for 20 ns. The production simulation was carried out with the NVT ensemble at 298.2 K for 5 ns. VMD<sup>53</sup> software was used to visualize the systems and obtain the ion association state. Anions and cations were treated as an association if their center distance was less than 2.4 Å.

**2.3. Electrochemical Measurements and Material Characterizations.** An electrochemical workstation (CHI1030C) was used to verify the electrochemical window of different electrolytes. Linear scanning voltammetry (LSV) test was performed at 3.0–5.0 V for the electrochemical window of electrolytes. SP-PVDF-Al ( $1.2 \times 1.2 \text{ cm}^2$ ) was chosen as a working electrode and lithium metal was regarded as a counter electrode and reference electrode, with a scanning speed of  $0.1 \text{ mV s}^{-1}$ . Cyclic voltammetry (CV) of LillNCM523 cells was performed at  $0.1 \text{ mV s}^{-1}$  under 3–4.3 V for 2.5 cycles, followed by chronoamperometry (CA) test at 4.3 V for 10 h. The NCM523 cathode ( $1.2 \times 1.2 \text{ cm}^2$ ) was chosen as the working electrode and lithium metal was regarded as a counter electrode and reference electrode.

All cells were CR-2016 type assembled with 80  $\mu\text{L}$  electrolyte, Celgard2500 and the electrode materials mentioned above in a glovebox. The Neware test system was used to study the charging and discharging behaviors of cells in different electrolytes. Room-temperature and low-temperature LillNCM523 cells were formed by 0.1C (4.3 V, 1C = 160  $\text{mAh g}^{-1}$  or 4.5 V, 1C = 180  $\text{mAh g}^{-1}$ ) for one cycle at 25 °C. The room-temperature cells were constant current/constant voltage charged and constant current discharged at 0.5C (the current of constant voltage charge is 1/10 of constant current charge). The low-temperature LillNCM523 cells were discharged at 0.1C under different temperatures after room-temperature formation. High-temperature LillNCM523 cells were formed by 0.1C at 60 °C, then constant current/constant voltage charged and constant current discharged at 0.5C and 1C, respectively. A third method reported by Adams et al.<sup>54</sup> was used to test the coulombic efficiency (CE) of Lill Cu cells at  $0.5 \text{ mA cm}^{-2}$ . First, 5  $\text{mAh cm}^{-2}$  lithium was deposited and stripped on Cu for precycling. Second, 5  $\text{mAh cm}^{-2}$  lithium was deposited on Cu as a Li reservoir ( $Q_t$ ). Then, 1  $\text{mAh cm}^{-2}$  ( $Q_c$ ) lithium was deposited and stripped for 10 cycles. Finally, the cells were charged to 1 V to strip all of the remaining lithium. The calculation formula of CE was as follows

$$\text{CE} = \left( \frac{n \times Q_c + Q_s}{n \times Q_c + Q_t} \right) \times 100\% \quad (2)$$

$n$  is the number of cycles (here 10) and  $Q_s$  is the final charge capacity.

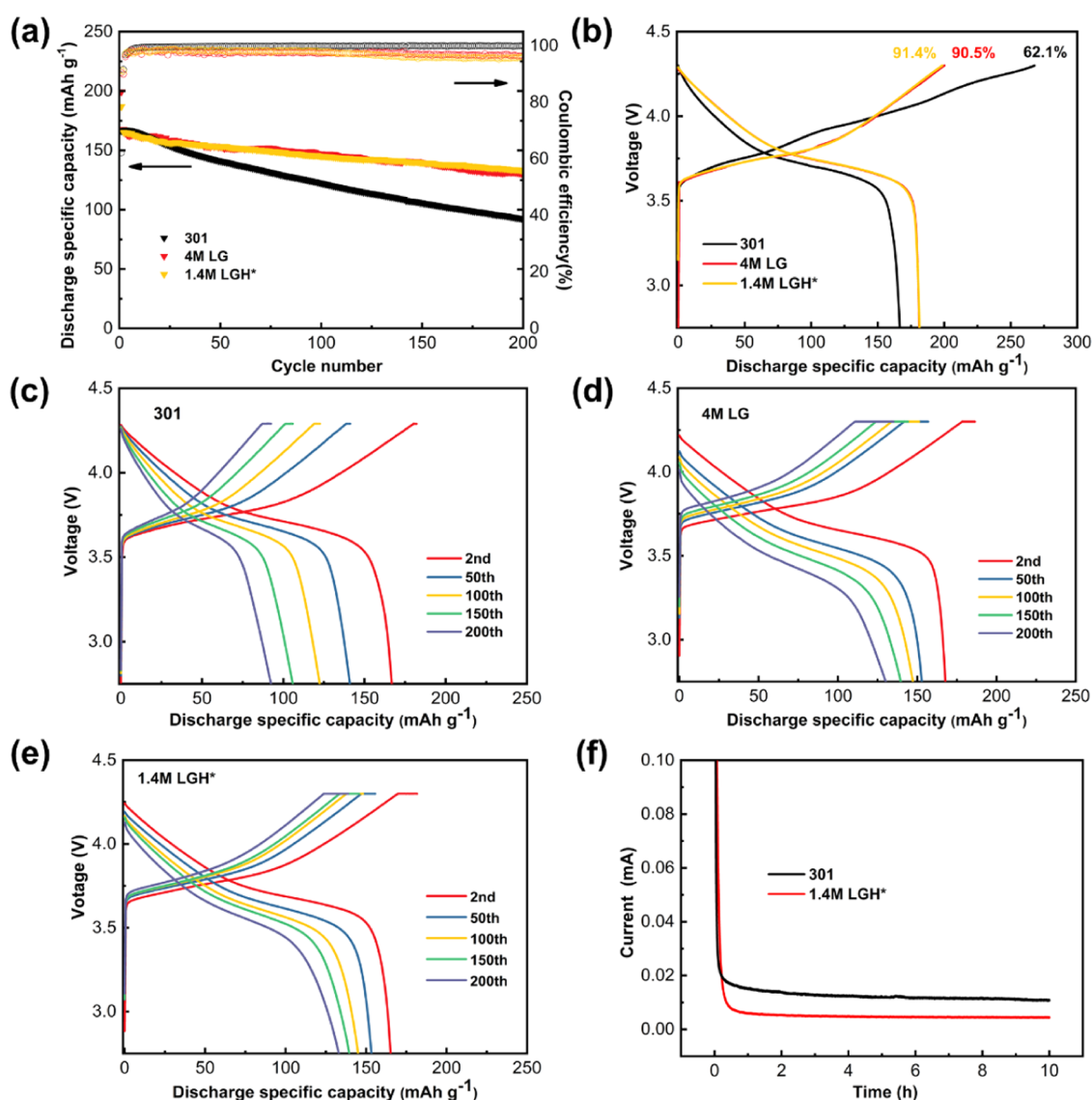


**Figure 2.** Electrochemical performance of Li||NCM523 batteries under 2.75–4.3 V (60 °C). (a) Cyclic performance of three electrolytes after 200 cycles. Voltage-specific capacity curves of (b) first cycle in different electrolytes, (c) 301, (d) 4M LG, and (e) 1.4M LGH\*. (f) Chronoamperometry (CA) test of two electrolytes at 4.3 V for 10 h.

The solvent structures of different concentrations of electrolytes were verified by  $^7\text{Li-NMR}$  (nuclear magnetic resonance lithium spectrum) (Ascend 500 MHz spectrometer) at 25 °C. After cycling, Li||NCM523 cells were disassembled and electrodes were drip washed three times (DMC used for electrodes in 301, DME used for electrodes in self-prepared electrolytes). A scanning electron microscope (SEM) (Zeiss Gemini SEM 500) was used to observe the morphological changes in the NCM523 material and lithium metal. Energy-dispersive X-ray spectroscopy (EDS) was used for detecting lithium metal. The changes in the NCM523 materials were investigated by X-ray diffraction (XRD) (Rigaku Miniflex 600 X-ray diffractometer). The target of XRD was Cu K $\alpha$  and the test speed was  $5^\circ \text{ min}^{-1}$ , ranging from 10 to  $90^\circ$ . The morphology of CEI and lattice changes of the NCM523 cathode were characterized by a transmission electron microscope (TEM) (JEM2100, JEM30). The photoelectronic energy spectrum (XPS) (PHI Quantum 2000) was used to analyze the composition of the CEI. Differential scanning calorimetry (DSC) (STA 449 F3 Jupiter) was used to study the thermal stability of two lithium salts. The conductivity of all electrolytes was measured by a conductivity meter (DSC-307A) and viscosity was measured by a viscometer (VM-10A-L). The contact

angle was obtained by a contact angle tester (JC-2000C1). The above experiments were carried out at 25 °C.

### 3. RESULTS AND DISCUSSION

**3.1. Physicochemical Properties of Electrolyte.** Firstly, the thermal stability of pure LiDfP and LiPF $_6$  was tested by DSC. As expected, the decomposition temperature of LiDfP was about 350 °C, which was higher than that of LiPF $_6$  (Figure S1). The results of the density functional theory (DFT) and linear scanning voltammetry (LSV) (Figures 1a and S2) demonstrate that the antioxidation of electrolytes can be enhanced by increasing the lithium salt concentration. However, the application of a high-concentration electrolyte is limited by its high viscosity and high cost. Among all HCEs, 4M LiDfP-G4 (4M LG) had the optimal electrochemical performance and suitable physicochemical properties. Therefore, different proportions of HFE were added to 4M LG for dilution. After dilution, the viscosity was significantly reduced and the wettability with the Celgard separator was improved (Figure S3). The conductivity was slightly reduced due to the

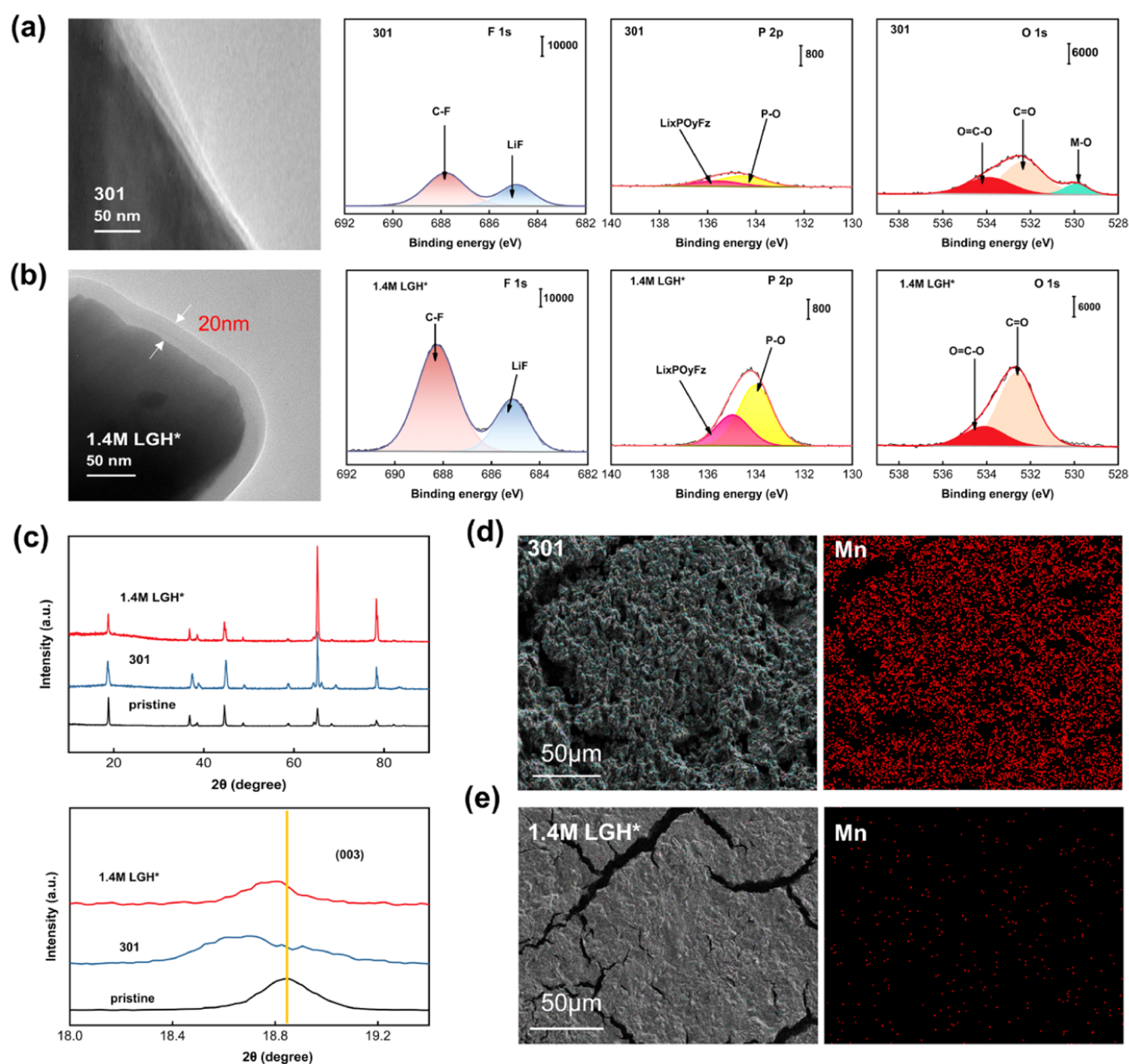


**Figure 3.** Material characterizations of the electrodes after cycling under 4.3 V (60 °C). TEM tests and XPS (F 1s, O 1s, P 2p) results of NCM523 after 10 cycles in (a) 301 and (b) 1.4M LGH\*. (c) XRD test of the NCM523 cathode after 200 cycles. SEM-EDS mapping images of lithium metal after 200 cycles in (d) 301 and (e) 1.4M LGH\*.

low dielectric constant of the HFE. The solvation structure of different electrolytes around  $\text{Li}^+$  was studied by  $^7\text{Li}$ -NMR (Figure 1b). From the 1M LG electrolyte to the 6M LG electrolyte, the chemical shift moved to higher fields, indicating stronger solvated structures around the  $\text{Li}^+$  ions. In addition, the chemical shift of the 1.4M LGH electrolyte was similar to that of 4M LG but different from that of 1.4M LG, indicating that the addition of HFE did not change the solvation structure. The result of molecular dynamics calculation (MD) was consistent with  $^7\text{Li}$ -NMR (Figure 1c–g and Tables S2–S5). The coordination number of  $\text{Li}^+$  with  $\text{PO}_2\text{F}_2^-$  is about 2 in a primary solvation sheath (within 2.4 Å), implying the AGG solvation structure of 4M LG. In 1.4M LGH, the coordination number of  $\text{PO}_2\text{F}_2^-$  with  $\text{Li}^+$  remained at 2 and the number of HFE- $\text{Li}^+$  was about 0, indicating no influence of

HFE on the solvation structure.<sup>31</sup> In addition, the ratio of free G4 (that did not bind to  $\text{Li}^+$ ) was decreased from 70.3% (in 1.4M LG) to 40.1% (in 1.4M LGH) (Figure S4), in harmony with a higher oxidation potential. The  $\text{Li}^+$ –solvents,  $\text{Li}^+$ –anions, and solvents–solvents of different electrolytes could be seen visually from the molecular dynamics snapshot (Figure 1g). In general, the combination of LiDFP and LHCE could generate an anion-based solvation structure with less amount of free solvents.

**3.2. High Temperature.** Li||NCM523 cells were charged to 4.3 V to test the electrochemical performance of the above electrolytes under 60 °C (Figures 2 and S5). The capacity retention was compared with the discharge capacity of the second cycle (more details in the Experimental Section). The cell in 301 delivered 55.4% capacity after 200 cycles (Figure

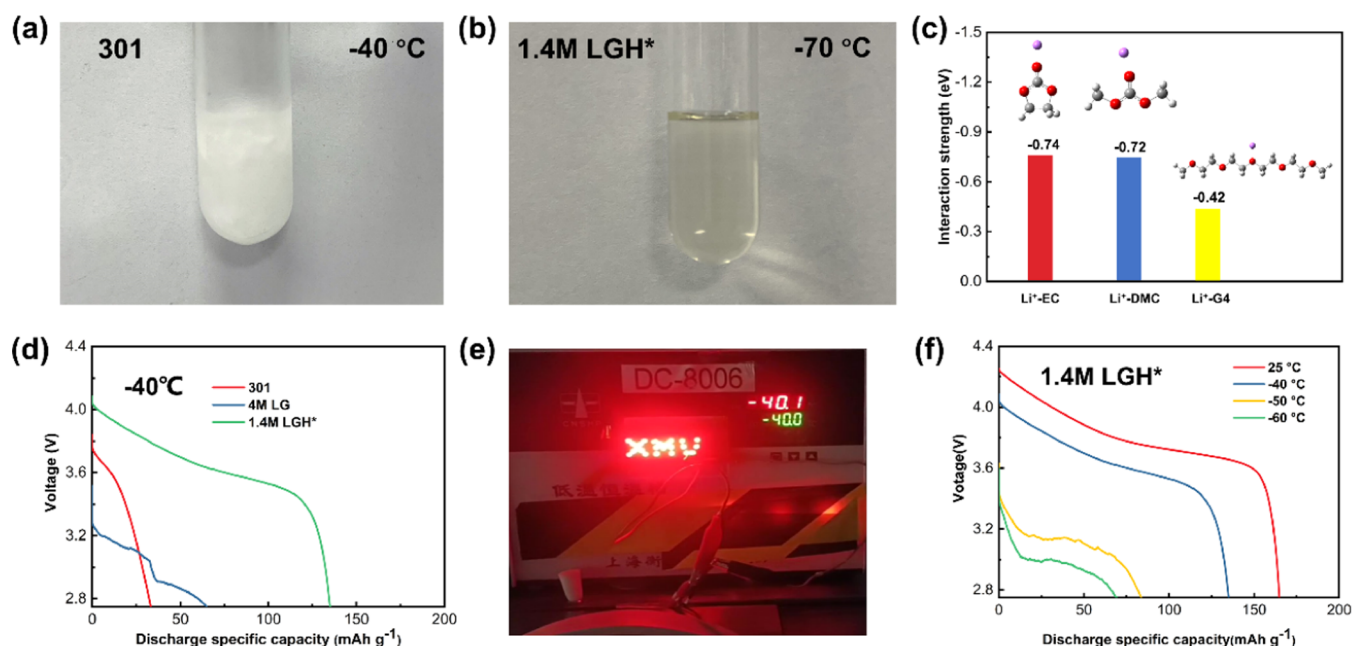


**Figure 4.** Digital image of (a) 301 after keeping at  $-40^{\circ}\text{C}$  for 1 h and (b) 1.4M LGH\* after keeping at  $-70^{\circ}\text{C}$  for 1 h. (c) Binding energy ( $E_b$ ) of different solvents and  $\text{Li}^+$ . (d) Voltage-specific capacity curves of 4.3 V LillNCMS523 batteries in the three electrolytes under  $-40^{\circ}\text{C}$ . (e) LillNCMS523 cell powers LED bulbs at  $-40^{\circ}\text{C}$ . (f) Voltage-specific capacity curves of 4.3 V LillNCMS523 batteries in 1.4M LGH\* under different temperatures.

2a–c), along with 62.1% initial Coulombic efficiency (ICE) at 0.1C. The ICE of the cell in 4M LG was 90.5% higher than that in 301, but only 77.8% of the initial capacity was released after 200 cycles due to high polarization voltage (Figure 2d), which could be due to the high viscosity of the electrolyte. After dilution, the cycling performance of the cell in 1.4M LGH\* was indeed improved, remaining at 81.0% capacity retention after 200 cycles (Figure 2e). In addition, the rate performance of cells in 1.4M LGH\* was also improved (Figure S6), and the electrochemical performance of the LillNCMS523 full cell was also investigated (Figure S7). Finally, the residual current of the cell in 1.4M LGH\* was smaller than that of 301 in the CA test under 4.3 V (Figure 2f, after the CV test in Figure S8), indicating that the side reactions were effectively suppressed.

The cyclic performance of LillNCMS523 cells and the structure of materials were affected by the CEI formed on the NCM523 cathode. Hence, TEM and XPS were carried out to analyze the morphology and composition of NCM523 after 10 cycles at  $60^{\circ}\text{C}$  in different electrolytes. Figure 3a shows an uneven CEI on the cathode surface after cycling in 301, which might be due to constant decomposition of the electrolyte at a high temperature. Also, it was found that all samples contained similar components such as acetylene black (C–C, 284.8 eV, C 1s) and PVDF (CF<sub>2</sub>–CH<sub>2</sub>, 285.5 eV, C–F, 291.1 eV, C 1s)<sup>55</sup> (Figure S9). In addition, more C–O and C=O species in the C 1s spectrum and less lithium fluoride (LiF, 684.9 eV, F 1s) were formed by the decomposition product of solvents. The continuous LiPF<sub>6</sub> decomposition at  $60^{\circ}\text{C}$  was identified by Li<sub>x</sub>PO<sub>y</sub>F<sub>z</sub> (134.62 eV, P 2p).<sup>56</sup> Therefore, the M–O peak (529.9 eV, O 1s) of TMIs was detected, implying that the CEI generated by the solvent was unstable and could not protect the cathode material.<sup>57</sup> However, after cycling in 1.4M LGH\*, a denser and uniform CEI of 20 nm thickness could be observed and no M–O signal was detected, implying that the CEI could effectively inhibit the dissolution of TMIs (Figure

3b). In addition, more LiF inorganic components were generated by PO<sub>2</sub>F<sub>2</sub><sup>−</sup>, improving the transmission of Li<sup>+</sup> on the interface.<sup>29</sup> In addition, more Li<sub>3</sub>PO<sub>4</sub> (P–O, 133.8 eV, P 2p) could help scavenge the TMIs,<sup>34</sup> in line with better cyclic performance.

To further verify the CEI protective effect, we disassembled the cells after 200 cycles and performed a variety of material characterization tests on both electrodes. As shown in Figure S10, the morphology of pristine cathode material was a secondary particle with a regular spherical shape. However, the NCM523 particles broke up seriously after cycling in 301, indicating that the unstable CEI on NCM523 could hardly protect the material from a side reaction with electrolyte during the cycles, which was consistent with the rapid capacity decline. Only a few particles broke up after cycling in 1.4M LGH\*, maintaining the complete structure. This is consistent with the stable CEI generated by anions.<sup>58</sup> The XRD test results of a totally discharged NCM523 cathode in two electrolytes are presented in Figure 3c, consistent with a typical layered structure.<sup>35</sup> The (003) peak in the XRD pattern of both positive electrodes shifted to a lower angle after 200 cycles, which was related to the extraction of Li<sup>+</sup> in layered cathode materials.<sup>59</sup> However, it was obvious that the positive electrode cycled in 301 shows a more negative shift than the electrode cycled in 1.4M LGH\*. This might be due to the enhanced reversibility of de-intercalation of lithium ions in 1.4M LGH\*. It was reported that the degradation of the cathode led to the serious dissolution of TMIs, which would migrate to the anode and cause crosstalk with dendritic lithium formation.<sup>33</sup> The surface morphology and the element distribution of lithium metal anode after 200 cycles in both electrolytes were analyzed by SEM and EDS mapping (Figure 3d,e). Less amount of F and P elements and a higher amount of transition-metal elements (especially Mn) were detected on the surface of lithium metal after 200 cycles in 301 (Figure S11). As shown in Figure 3d, the Mn<sup>2+</sup> was concentrated in the

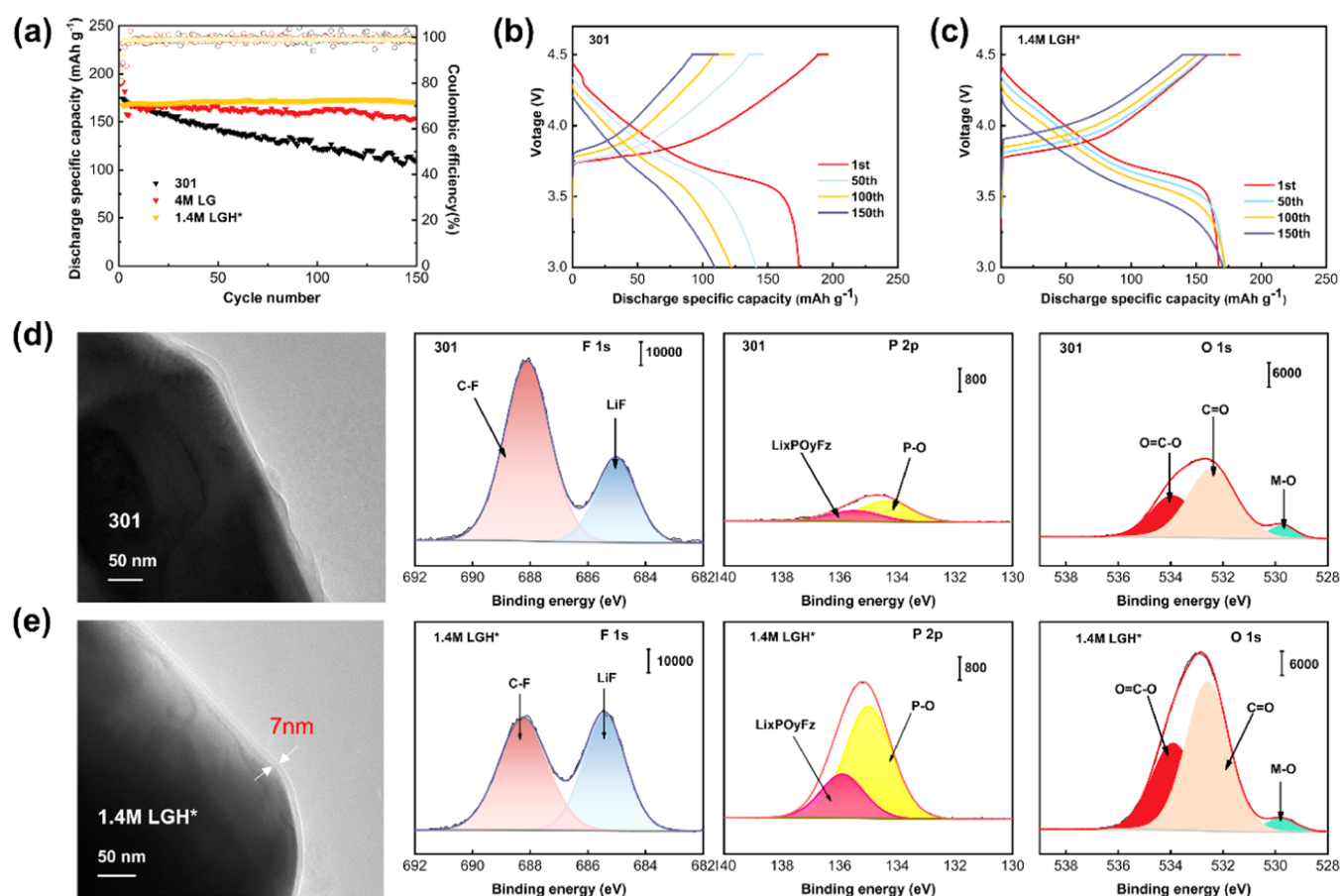


**Figure 5.** (a) Electrochemical performance of LillNCMS23 batteries under 3–4.5 V (25 °C). Voltage-specific capacity curves of LillNCMS23 batteries under 3–4.5 V (25 °C) with (b) 301 and (c) 1.4M LGH\*. TEM test and XPS (F 1s, O 1s, P 2p) results of NCM523 after 50 cycles in (d) 301 and (e) 1.4M LGH\*.

position where dendrite formats.<sup>33</sup> Conversely, the surface of lithium metal in the LHCE electrolyte was relatively dense (cracks might be affected by sample preparation), with no obvious TMI dissolution in Figure 3e. All in all, the electrodes were effectively protected by the CEI generated by the anion-based solvation structure, which was consistent with the good cyclic performance.

**3.3. Low Temperature.** LillNCMS23 cells were charged to 4.3 V and then discharged at different temperatures with 0.1C. The discharge capacities of LillNCMS23 batteries were about 168.9 mAh g<sup>-1</sup>. As can be seen from Figure 4a, 301 froze quickly after storage at -40 °C for 1h, while 1.4M LGH\* still remained liquid after storage at -70 °C (Figure 4b). The freezing point of the modified electrolyte was about -95 °C as tested by DSC (-120 to 100 °C) (Figure S12). Compared with those of the 301 electrolyte, the AGG solvation structure<sup>26</sup> of the 1.4M LGH\* electrolyte and the lower binding energy<sup>10</sup> (Figure 4c) between G4 and Li<sup>+</sup> were favorable for the desolvation processes, enabling better low-temperature performance. The low-temperature discharge performance of all electrolytes was tested at -40 °C (Figure 4d). The cell in 301 delivered almost no capacity due to solidification of electrolyte and the cell in 4M LiDFP-G4 only delivered 64.9 mAh g<sup>-1</sup> capacity. However, 1.4M LGH\* maintained 81.4% capacity of room temperature. Furthermore, the cell could light up LED bulbs at -40 °C and deliver 42.0% capacity of room temperature at -60 °C (Figure 4e,f).

Generally, the electrolyte showed good performance under low temperatures.

**3.4. High Voltage.** In addition, the performance of 4.5 V LillNCMS23 cells at 25 °C was also studied (Figures 5a–c and S13). The capacity retention could reach 98.5% in 1.4M LGH\* after 150 cycles, better than 63.7% in 301. The different cyclic performance under a high operating voltage may result from the CEI generated by different solvation structures. The CEI on the NCM523 cathode after 50 cycles in 301 was nonuniform with more C–O organic species generated by solvents (Figures 5d and S14). Inversely, the thin (~7 nm) CEI in 1.4M LGH\* was uniform with more LiF, which was similar to the CEI on the cathode at a high temperature and could effectively protect electrodes from parasitic reactions (Figure 5e). In addition, the Coulombic efficiency of LillCu was tested by method 3 (details in the Experimental Section) (Figure S15) and the CEI of the modified electrolyte was 97.0%, higher than 86.6% for 301, indicating better compatibility with lithium metal. In addition, the accumulation of dead lithium could be alleviated by 1.4M LGH\* (Figure S16).

The optimal CEI can ensure the integrity of the positive electrode under a high operating voltage. XRD of the discharged positive electrode in both electrolytes after 100 cycles are presented in Figure 6a. As mentioned above, the smaller shift of the (003) peak indicates that Li<sup>+</sup> can reintercalate into the structure of NCM523 in 1.4M LGH\* sufficiently. TEM is used to observe the phase transformation

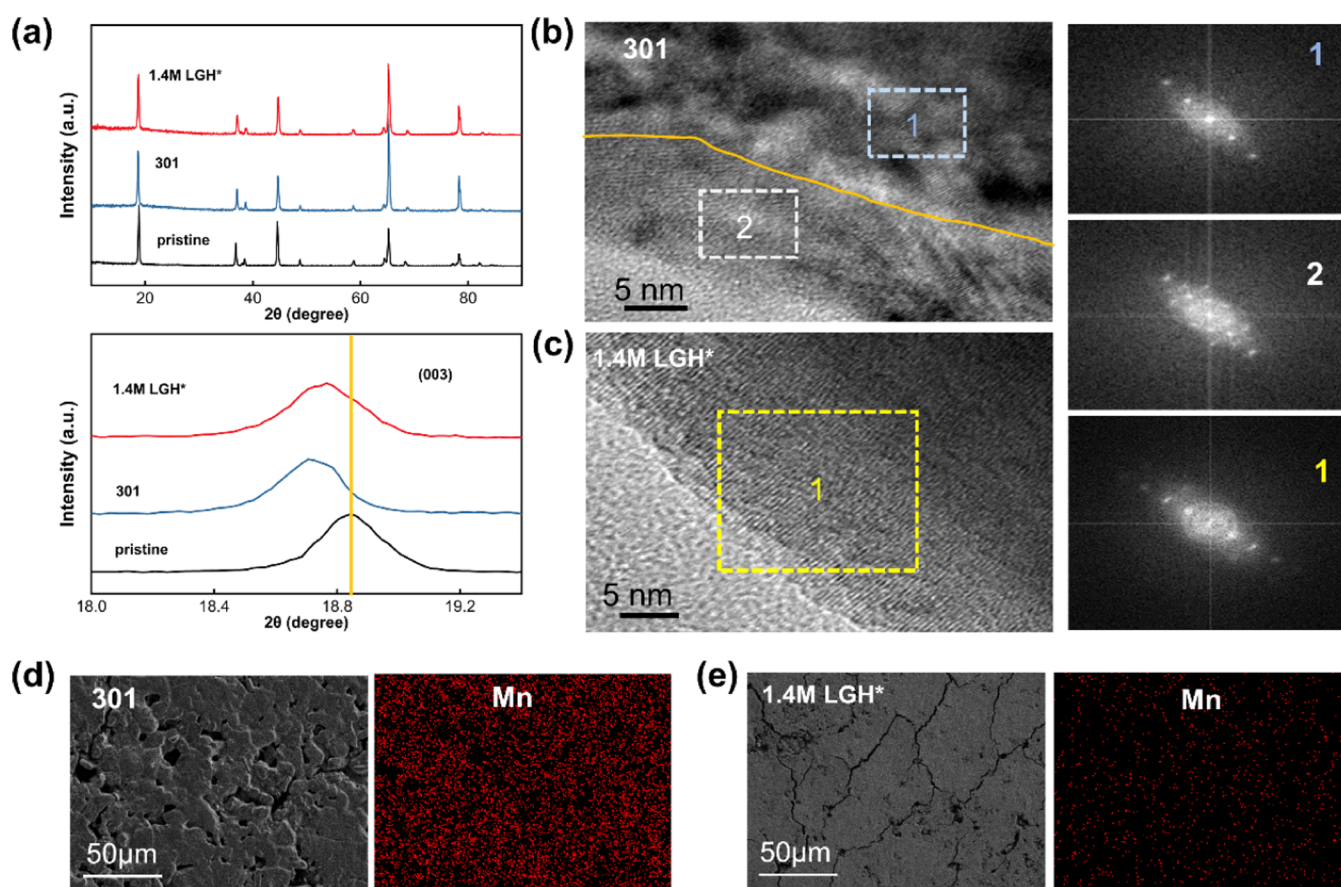


**Figure 6.** Material characterization of discharged electrodes after 100 cycles under 4.5 V (25 °C). (a) XRD of the NCM523 electrode. TEM images of the NCM523 electrode in (b) 301 and (c) 1.4M LGH\*. SEM-EDS mapping images of lithium metal in (d) 301 and (e) 1.4M LGH\*.

on the NCM523 cathode after 100 cycles. In 301, a rock salt phase with a thickness of 12 nm is detected in area 2 (Figure 6b). Nevertheless, the cycled NCM523 cathode in 1.4M LGH\* maintains the layered structure with no obvious phase transition (Figure 6c). In addition, fewer TMIs were detected on lithium in 1.4M LGH\* than that in 301 (Figures 6d,e and S17). Overall, the stable CEI derived from an anion-solvated structure can enable stable cycling of the batteries under a high temperature or a high operating voltage.

#### 4. CONCLUSIONS

The LiDfP-based local high-concentration electrolyte (1.4M LGH\*) in this work contains abundant CIPs and AGGs. This anion-based solvation structure can help generate a uniform CEI with plentiful LiF, P–O, isolating the constant side reactions between the electrolyte and the cathode and inhibiting the dissolution of TMIs. This modified CEI effectively improves the performance of LillNCM523 cells at a high temperature (60 °C) and a high voltage (4.5 V). In addition, this solvation structure can weaken the Li<sup>+</sup>–solvent interaction for accelerating the desolvation process, improving the low-temperature discharge capacity. All in all, the combination of LiDfP and localized high-concentration strategy is a promising way to design wide-temperature and high-voltage electrolytes in the future.

#### ASSOCIATED CONTENT

##### Supporting Information

The Supporting Information is available free of charge at <https://pubs.acs.org/doi/10.1021/acsami.2c02221>.

LSV, ion conductivity, and viscosity tests of different electrolytes under 25 °C; details of the theoretical calculation; electrochemical performance of 4.3 V Lill NCM523 cell in different HCEs (25 °C and 60 °C); CV of the LillNCM523 battery in two electrolytes; SEM, XPS, and EDS characterizations of electrodes cycled under 4.3V (60 °C); SEM, XPS, and EDS characterizations of electrodes cycled under 4.5V (25 °C); and performance of LillCu half-cells in 301, 1.4M LG, and 1.4M LGH\* electrolyte (25 °C) (PDF)

#### AUTHOR INFORMATION

##### Corresponding Authors

**Yang Yang** – State-Province Joint Engineering Laboratory of Power Source Technology for New Energy Vehicle, Engineering Research Center of Electrochemical Technology, Ministry of Education, College of Chemistry and Chemical Engineering, Xiamen University, Xiamen 361005, P. R. China; Email: [yangyang419@xmu.edu.cn](mailto:yangyang419@xmu.edu.cn)

**Jinbao Zhao** – State-Province Joint Engineering Laboratory of Power Source Technology for New Energy Vehicle, Engineering Research Center of Electrochemical Technology, Ministry of Education, College of Chemistry and Chemical Engineering, Xiamen University, Xiamen 361005, P. R.

China; [orcid.org/0000-0002-2753-7508](https://orcid.org/0000-0002-2753-7508);  
Email: [jbzhao@xmu.edu.cn](mailto:jbzhao@xmu.edu.cn)

## Authors

**Silan Kuang** – State-Province Joint Engineering Laboratory of Power Source Technology for New Energy Vehicle, Engineering Research Center of Electrochemical Technology, Ministry of Education, College of Chemistry and Chemical Engineering, Xiamen University, Xiamen 361005, P. R. China

**Haiming Hua** – State-Province Joint Engineering Laboratory of Power Source Technology for New Energy Vehicle, Engineering Research Center of Electrochemical Technology, Ministry of Education, College of Chemistry and Chemical Engineering, Xiamen University, Xiamen 361005, P. R. China

**Pengbin Lai** – State-Province Joint Engineering Laboratory of Power Source Technology for New Energy Vehicle, Engineering Research Center of Electrochemical Technology, Ministry of Education, College of Chemistry and Chemical Engineering, Xiamen University, Xiamen 361005, P. R. China

**Jialin Li** – State-Province Joint Engineering Laboratory of Power Source Technology for New Energy Vehicle, Engineering Research Center of Electrochemical Technology, Ministry of Education, College of Chemistry and Chemical Engineering, Xiamen University, Xiamen 361005, P. R. China

**Xiaodie Deng** – State-Province Joint Engineering Laboratory of Power Source Technology for New Energy Vehicle, Engineering Research Center of Electrochemical Technology, Ministry of Education, College of Chemistry and Chemical Engineering, Xiamen University, Xiamen 361005, P. R. China

Complete contact information is available at:  
<https://pubs.acs.org/10.1021/acsami.2c02221>

## Notes

The authors declare no competing financial interest.

## ACKNOWLEDGMENTS

The authors gratefully acknowledge the financial support of the National Key Research and Development Program of China (2017YFB0102000), the National Natural Science Foundation of China (21875198 and 22021001), the Fundamental Research Funds for the Central Universities (20720190040), the Natural Science Foundation of Fujian Province of China (2020J05009), and the Key Project of Science and Technology of Xiamen (3502Z20201013), and the Key R&D Program of Yunnan Province (No. 202103AA080019). Also, they are grateful to the Tan Kah Kee Innovation Laboratory (IKKEM) for help with XPS, NMR, and SEM.

## REFERENCES

- (1) Hou, J. B.; Yang, M.; Wang, D. Y.; Zhang, J. L. Fundamentals and Challenges of Lithium Ion Batteries at Temperatures between -40 and 60 °C. *Adv. Energy Mater.* **2020**, *10*, No. 1904152.
- (2) Zhang, N.; Deng, T.; Zhang, S.; Wang, C.; Chen, L.; Wang, C.; Fan, X. Critical review on low-temperature Li-ion/metal batteries. *Adv. Mater.* **2021**, No. e2107899.
- (3) Rodrigues, M.-T. F.; Babu, G.; Gullapalli, H.; Kalaga, K.; Sayed, F. N.; Kato, K.; Joyner, J.; Ajayan, P. M. A materials perspective on Li-

ion batteries at extreme temperatures. *Nat. Energy* **2017**, *2*, No. 17108.

- (4) Jeong, M.; Lee, W.; Yun, S.; Choi, W.; Park, H.; Lee, E.; Kim, J.; Cho, S. J.; Lee, N. H.; Shin, H. J.; Yoon, W. S. Strategic Approach to Diversify Design Options for Li-Ion Batteries by Utilizing Low-Ni Layered Cathode Materials. *Adv. Energy Mater.* **2021**, *12*, No. 2103052.

- (5) Chae, S.; Kwak, W.-J.; Han, K. S.; Li, S.; Engelhard, M. H.; Hu, J.; Wang, C.; Li, X.; Zhang, J.-G. Rational Design of Electrolytes for Long-Term Cycling of Si Anodes over a Wide Temperature Range. *ACS Energy Lett.* **2021**, *6*, 387–394.

- (6) Fan, X. L.; Ji, X.; Chen, L.; Chen, J.; Deng, T.; Han, F. D.; Yue, J.; Piao, N.; Wang, R. X.; Zhou, X. Q.; Xiao, X. Z.; Chen, L. X.; Wang, C. S. All-temperature batteries enabled by fluorinated electrolytes with non-polar solvents. *Nat. Energy* **2019**, *4*, 882–890.

- (7) Liu, M.; Vatamanu, J.; Chen, X.; Xing, L.; Xu, K.; Li, W. Hydrolysis of LiPF<sub>6</sub>-Containing Electrolyte at High Voltage. *Adv. Energy Mater.* **2021**, *6*, 2096–2102.

- (8) Zhou, R.; Huang, J.; Lai, S.; Li, J.; Wang, F.; Chen, Z.; Lin, W.; Li, C.; Wang, J.; Zhao, J. A bifunctional electrolyte additive for H<sub>2</sub>O/HF scavenging and enhanced graphite/LiNi<sub>0.5</sub>Co<sub>0.2</sub>Mn<sub>0.3</sub>O<sub>2</sub> cell performance at a high voltage. *Sustainable Energy Fuels* **2018**, *2*, 1481–1490.

- (9) Kafle, J.; Harris, J.; Chang, J.; Koshina, J.; Boone, D.; Qu, D. Development of wide temperature electrolyte for graphite/LiNiMnCoO<sub>2</sub> Li-ion cells: High throughput screening. *J. Power Sources* **2018**, *392*, 60–68.

- (10) Wang, Z. X.; Sun, Z. H.; Shi, Y.; Qi, F. L.; Gao, X. N.; Yang, H. C.; Cheng, H. M.; Li, F. Ion-Dipole Chemistry Drives Rapid Evolution of Li Ions Solvation Sheath in Low-Temperature Li Batteries. *Adv. Energy Mater.* **2021**, *11*, No. 2100935.

- (11) Xu, K. Electrolytes and interphases in Li-ion batteries and beyond. *Chem. Rev.* **2014**, *114*, 11503–11618.

- (12) Fan, X.; Wang, C. High-voltage liquid electrolytes for Li batteries: progress and perspectives. *Chem. Soc. Rev.* **2021**, *50*, 10486–10566.

- (13) Zhao, Q.; Liu, X.; Zheng, J.; Deng, Y.; Warren, A.; Zhang, Q.; Archer, L. Designing electrolytes with polymerlike glass-forming properties and fast ion transport at low temperatures. *Proc. Natl. Acad. Sci. U.S.A.* **2020**, *117*, 26053–26060.

- (14) Thenuwara, A. C.; Shetty, P. P.; McDowell, M. T. Distinct Nanoscale Interphases and Morphology of Lithium Metal Electrodes Operating at Low Temperatures. *Nano Lett.* **2019**, *19*, 8664–8672.

- (15) Li, Q.; Jiao, S.; Luo, L.; Ding, M. S.; Zheng, J.; Cartmell, S. S.; Wang, C. M.; Xu, K.; Zhang, J. G.; Xu, W. Wide-Temperature Electrolytes for Lithium-Ion Batteries. *ACS Appl. Mater. Interfaces* **2017**, *9*, 18826–18835.

- (16) Ren, X.; Zhang, X.; Shadik, Z.; Zou, L.; Jia, H.; Cao, X.; Engelhard, M. H.; Matthews, B. E.; Wang, C.; Arey, B. W.; Yang, X. Q.; Liu, J.; Zhang, J. G.; Xu, W. Designing Advanced In Situ Electrode/Electrolyte Interphases for Wide Temperature Operation of 4.5 V LillLiCoO<sub>2</sub> Batteries. *Adv. Mater.* **2020**, *32*, No. e2004898.

- (17) Xiao, P.; Luo, R.; Piao, Z.; Li, C.; Wang, J.; Yu, K.; Zhou, G.; Cheng, H.-M. High-Performance Lithium Metal Batteries with a Wide Operating Temperature Range in Carbonate Electrolyte by Manipulating Interfacial Chemistry. *ACS Energy Lett.* **2021**, *6*, 3170–3179.

- (18) Xiao, Y.; Xu, R.; Xu, L.; Ding, J.-F.; Huang, J.-Q. Recent advances in anion-derived SEIs for fast-charging and stable lithium batteries. *Energy Mater.* **2021**, *1*, No. 100013.

- (19) Yang, Y.; Yin, Y.; Davies, D. M.; Zhang, M.; Mayer, M.; Zhang, Y.; Sablina, E. S.; Wang, S.; Lee, J. Z.; Borodin, O.; Rustomji, C. S.; Meng, Y. S. Liquefied gas electrolytes for wide-temperature lithium metal batteries. *Energy Environ. Sci.* **2020**, *13*, 2209–2219.

- (20) Rustomji, C. S.; Yang, Y.; Kim, T. K.; Mac, J.; Kim, Y. J.; Caldwell, E.; Chung, H.; Meng, Y. S. Liquefied gas electrolytes for electrochemical energy storage devices. *Science* **2017**, *356*, No. eaal4263.

- (21) Cheng, H.; Sun, Q.; Li, L.; Zou, Y.; Wang, Y.; Cai, T.; Zhao, F.; Liu, G.; Ma, Z.; Wahyudi, W.; Li, Q.; Ming, J. Emerging Era of Electrolyte Solvation Structure and Interfacial Model in Batteries. *ACS Energy Lett.* **2022**, *7*, 490–513.
- (22) Chen, X.; Zhang, X.-Q.; Li, H.-R.; Zhang, Q. Cation–Solvent, Cation–Anion, and Solvent–Solvent Interactions with Electrolyte Solvation in Lithium batteries. *Batteries Supercaps* **2019**, *2*, 114.
- (23) Zhang, L.; Chen, Y. Electrolyte solvation structure as a stabilization mechanism for electrodes. *Energy Mater.* **2021**, *1*, No. 100004.
- (24) Zheng, T.; Xiong, J.; Shi, X.; Zhu, B.; Cheng, Y.-J.; Zhao, H.; Xia, Y. Cocktail therapy towards high temperature/high voltage lithium metal battery via solvation sheath structure tuning. *Energy Storage Mater.* **2021**, *38*, 599–608.
- (25) Zou, Y.; Cao, Z.; Zhang, J.; Wahyudi, W.; Wu, Y.; Liu, G.; Li, Q.; Cheng, H.; Zhang, D.; Park, G. T.; Cavallo, L.; Anthopoulos, T. D.; Wang, L.; Sun, Y. K.; Ming, J. Interfacial Model Deciphering High-Voltage Electrolytes for High Energy Density, High Safety, and Fast-Charging Lithium-Ion Batteries. *Adv. Mater.* **2021**, *33*, No. e2102964.
- (26) Holoubek, J.; Liu, H.; Wu, Z.; Yin, Y.; Xing, X.; Cai, G.; Yu, S.; Zhou, H.; Pascal, T. A.; Chen, Z.; Liu, P. Tailoring Electrolyte Solvation for Li Metal Batteries Cycled at Ultra-Low Temperature. *Nat. Energy* **2021**, *6*, 303–313.
- (27) Lin, X.; Salari, M.; Arava, L. M.; Ajayan, P. M.; Grinstaff, M. W. High temperature electrical energy storage: advances, challenges, and frontiers. *Chem. Soc. Rev.* **2016**, *45*, 5848–5887.
- (28) Wang, Z. X.; Qi, F. L.; Yin, L. C.; Shi, Y.; Sun, C. G.; An, B. G.; Cheng, H. M.; Li, F. An Anion-Tuned Solid Electrolyte Interphase with Fast Ion Transfer Kinetics for Stable Lithium Anodes. *Adv. Energy Mater.* **2020**, *10*, No. 1903843.
- (29) Pham, T. D.; Bin Faheem, A.; Chun, S. Y.; Rho, J. R.; Kwak, K.; Lee, K. K. Synergistic Effects on Lithium Metal Batteries by Preferential Ionic Interactions in Concentrated Bisalt Electrolytes. *Adv. Energy Mater.* **2021**, *11*, No. 2003520.
- (30) Yamada, Y.; Yamada, A. Review—Superconcentrated Electrolytes for Lithium Batteries. *J. Electrochem. Soc.* **2015**, *162*, A2406–A2423.
- (31) Wang, J.; Yamada, Y.; Sodeyama, K.; Chiang, C. H.; Tateyama, Y.; Yamada, A. Superconcentrated electrolytes for a high-voltage lithium-ion battery. *Nat. Commun.* **2016**, *7*, No. 12032.
- (32) Shanguan, X.; Xu, G.; Cui, Z.; Wang, Q.; Du, X.; Chen, K.; Huang, S.; Jia, G.; Li, F.; Wang, X.; Lu, D.; Dong, S.; Cui, G. Additive-Assisted Novel Dual-Salt Electrolyte Addresses Wide Temperature Operation of Lithium-Metal Batteries. *Small* **2019**, *15*, No. e1900269.
- (33) Klein, S.; Barmann, P.; Beuse, T.; Borzutzki, K.; Frerichs, J. E.; Kasnatscheew, J.; Winter, M.; Placke, T. Exploiting the Degradation Mechanism of NCM523 parallel Graphite Lithium-Ion Full Cells Operated at High Voltage. *ChemSusChem* **2021**, *14*, 595–613.
- (34) Klein, S.; Harte, P.; Henschel, J.; Bärmann, P.; Borzutzki, K.; Beuse, T.; Wickeren, S.; Heidrich, B.; Kasnatscheew, J.; Nowak, S.; Winter, M.; Placke, T. On the Beneficial Impact of  $\text{Li}_2\text{CO}_3$  as Electrolyte Additive in NCM523||Graphite Lithium Ion Cells Under High-Voltage Conditions. *Adv. Energy Mater.* **2021**, *11*, No. 2003756.
- (35) Liu, W.; Wang, M.; Chen, J.; Zhang, X.; Zhou, H. Synthesis of  $\text{LiNi}_{0.5}\text{Co}_{0.2}\text{Mn}_{0.3}\text{O}_2$  for Lithium Ion Batteries and the Mechanism of Capacity Fading at High Temperature. *J. Electrochem. Soc.* **2012**, *18* (2), 119–124.
- (36) Yoshida, K.; Nakamura, M.; Kazue, Y.; Tachikawa, N.; Tsuzuki, S.; Seki, S.; Dokko, K.; Watanabe, M. Oxidative-stability enhancement and charge transport mechanism in glyme-lithium salt equimolar complexes. *J. Am. Chem. Soc.* **2011**, *133*, 13121–13129.
- (37) Yamada, Y.; Wang, J.; Ko, S.; Watanabe, E.; Yamada, A. Advances and issues in developing salt-concentrated battery electrolytes. *Nat. Energy* **2019**, *4*, 269–280.
- (38) Cao, X.; Gao, P.; Ren, X.; Zou, L.; Engelhard, M. H.; Matthews, B. E.; Hu, J.; Niu, C.; Liu, D.; Arey, B. W.; Wang, C.; Xiao, J.; Liu, J.; Xu, W.; Zhang, J. G. Effects of fluorinated solvents on electrolyte solvation structures and electrode/electrolyte interphases for lithium metal batteries. *Proc. Natl. Acad. Sci. U.S.A.* **2021**, *118*, No. e2020357118.
- (39) Cao, X.; Jia, H.; Xu, W.; Zhang, J.-G. Review—Localized High-Concentration Electrolytes for Lithium Batteries. *J. Electrochem. Soc.* **2021**, *168*, No. 010522.
- (40) Bogle, X.; Vazquez, R.; Greenbaum, S.; Cresce, A.; Xu, K. Understanding  $\text{Li}^+$ -Solvent Interaction in Nonaqueous Carbonate Electrolytes with  $^{17}\text{O}$  NMR. *J. Phys. Chem. Lett.* **2013**, *4*, 1664–1668.
- (41) *Gaussian 09*, Revision E. 01, Frisch, M. J.; Trucks, G. W.; Fox, D. J., Eds.; Gaussian, Inc.: Wallingford CT, 2013.
- (42) Stephens, P. J.; Devlin, F. J.; Chabalowski, C. F.; Frisch, M. J. Ab-Initio Calculation of Vibrational Absorption and Circular-Dichroism Spectra Using Density-Functional Force-Fields. *J. Phys. Chem. A* **1994**, *98*, 11623–11627.
- (43) Krishnan, R.; Binkley, J. S.; Seeger, R.; Pople, J. A. Self-consistent molecular orbital methods. XX. A basis set for correlated wave functions. *J. Chem. Phys.* **1980**, *72*, 650–654.
- (44) Clark, T. C.; Chandrasekhar, J.; Spitznagel, G. W.; Schleyer, P. V. R. Efficient Diffuse Function-Augmented Basis Sets for Anion Calculations. III.\* The 3-21+G Basis Set for First-Row Elements, Li–F. *J. Comput. Chem.* **1983**, *4*, 294–301.
- (45) Marenich, A. V.; Cramer, C. J.; Truhlar, D. G. Universal solvation model based on solute electron density and on a continuum model of the solvent defined by the bulk dielectric constant and atomic surface tensions. *J. Phys. Chem. B* **2009**, *113*, 6378–6396.
- (46) Abraham, M. J.; Murtola, T.; Schulz, R.; Páll, S.; Smith, J. C.; Hess, B.; Lindahl, E. GROMACS: High performance molecular simulations through multi-level parallelism from laptops to supercomputers. *SoftwareX* **2015**, *1–2*, 19–25.
- (47) Jorgensen, W. L.; Maxwell, D. S.; Tirado-Rives, J. Development and Testing of the OPLS All-Atom Force Field on Conformational Energetics and Properties of Organic Liquids. *J. Am. Chem. Soc.* **1996**, *118*, 11225–11236.
- (48) Anderson, P. M.; Wilson, M. R. Developing a force field for simulation of poly(ethylene oxide) based upon ab initio calculations of 1,2-dimethoxyethane. *Mol. Phys.* **2005**, *103*, 89–97.
- (49) Shimizu, K.; Almantariotis, D.; Gomes, M. F. C.; Pádua, A. A.; Canongia Lopes, J. N. Molecular Force Field for Ionic Liquids V: Hydroxyethylimidazolium, Dimethoxy-2Methylimidazolium, and Fluoroalkylimidazolium Cations and Bis(Fluorosulfonyl)Amide, Perfluoroalkanesulfonylamide, and Fluoroalkylfluorophosphate Anions. *J. Phys. Chem. B* **2010**, *114*, 3592–3600.
- (50) Saito, S.; Watanabe, H.; Ueno, K.; Mandai, T.; Seki, S.; Tsuzuki, S.; Kameda, Y.; Dokko, K.; Watanabe, M.; Umehayashi, Y.  $\text{Li}^+$  Local Structure in Hydrofluoroether Diluted Li-Glyme Solvate Ionic Liquid. *J. Phys. Chem. B* **2016**, *120*, 3378–3387.
- (51) Park, C.; Kanduč, M.; Chudoba, R.; Ronneburg, A.; Risse, S.; Ballauff, M.; Dzubiella, J. Molecular simulations of electrolyte structure and dynamics in lithium–sulfur battery solvents. *J. Power Sources* **2018**, *373*, 70–78.
- (52) Martínez, L.; Andrade, R.; Birgin, E. G.; Martínez, J. M. PACKMOL: A Package for Building Initial Configurations for Molecular Dynamics Simulations. *J. Comput. Chem.* **2009**, *30*, 2157–2164.
- (53) Humphrey, W.; Dalke, A.; Schulten, K. VMD: Visual Molecular Dynamics. *J. Mol. Graphics* **1996**, *14*, 33–38.
- (54) Adams, B. D.; Zheng, J.; Ren, X.; Xu, W.; Zhang, J. G. Accurate Determination of Coulombic Efficiency for Lithium Metal Anodes and Lithium Metal Batteries. *Adv. Energy Mater.* **2017**, *8*, No. 1702097.
- (55) Ren, X.; Zou, L.; Cao, X.; Engelhard, M. H.; Liu, W.; Burton, S. D.; Lee, H.; Niu, C.; Matthews, B. E.; Zhu, Z.; Wang, C.; Arey, B. W.; Xiao, J.; Liu, J.; Zhang, J.-G.; Xu, W. Enabling High-Voltage Lithium-Metal Batteries under Practical Conditions. *Joule* **2019**, *3*, 1662–1676.
- (56) Zhang, X.; Zou, L.; Xu, Y.; Cao, X.; Engelhard, M. H.; Matthews, B. E.; Zhong, L.; Wu, H.; Jia, H.; Ren, X.; Gao, P.; Chen, Z.; Qin, Y.; Kompella, C.; Arey, B. W.; Li, J.; Wang, D.; Wang, C.; Zhang, J. G.; Xu, W. Advanced Electrolytes for Fast-Charging High-

Voltage Lithium-Ion Batteries in Wide-Temperature Range. *Adv. Energy Mater.* **2020**, *10*, No. 2070098.

(57) Lin, S.; Hua, H.; Li, Z.; Zhao, J. Functional Localized High-Concentration Ether-Based Electrolyte for Stabilizing High-Voltage Lithium-Metal Battery. *ACS Appl. Mater. Interfaces* **2020**, *12*, 33710–33718.

(58) Lin, S.; Hua, H.; Lai, P.; Zhao, J. A Multifunctional Dual-Salt Localized High-Concentration Electrolyte for Fast Dynamic High-Voltage Lithium Battery in Wide Temperature Range. *Adv. Energy Mater.* **2021**, *11*, No. 2101775.

(59) Li, J.; Huang, J.; Kong, X.; Zeng, J.; Zhao, J. The apparent capacity decay by kinetic degradation of  $\text{LiNi}_{0.5}\text{Co}_{0.2}\text{Mn}_{0.3}\text{O}_2$  during cycling under the high upper-limit charging potential. *J. Power Sources* **2021**, *496*, No. 229856.